IEEE Access
Multidisciplinary ⋮ Rapid Review ⋮ Open Access Journal

Received 28 November 2023, accepted 12 December 2023, date of publication 19 December 2023,
date of current version 26 December 2023.

Digital Object Identifier 10.1109/ACCESS.2023.3344578

RESEARCH ARTICLE

Real-Time Local Obstacle Avoidance and Trajectory Tracking Control of Quadrotor UAVs With Suspended Payload in Complex Environments

ZIYOU ZHANG, DONG ZHANG, DEZHI KONG, AND YANQIAN WANG
School of Information and Control Engineering, Qingdao University of Technology, Qingdao 266520, China
Corresponding author: Dong Zhang (zhangdong@qut.edu.cn)

ABSTRACT Compared with traditional vehicle transportation methods, unmanned aerial vehicles (UAVs) have many advantages in transporting cargo because they are not limited by factors such as road traffic. To address practical applications, this paper presents a local obstacle avoidance control scheme for the quadrotor with suspended payload, which is suitable for complex environments with dense obstacles and external disturbances. Firstly, the overall dynamic model of the quadrotor-payload system is established using Euler-Lagrange equations. Secondly, considering the envelope circle radius switching problem caused by changes in the amplitude of the swing angles of the payload, an obstacle avoidance constraint of the quadrotor-payload system is presented, and an R-function is introduced to improve the traditional artificial potential field method, so as to achieve a less conservative obstacle avoidance. Thirdly, a cascade control scheme based on sliding mode algorithm is designed for the quadrotor-payload system trajectory tracking under external disturbances. Moreover, to avoid payload oscillations during flight, a feed-forward controller is designed to suppress the swing of the payload. Finally, simulation results verify the effectiveness and superiority of the proposed local obstacle avoidance strategy and control scheme.

INDEX TERMS Artificial potential field, feed-forward control, obstacle avoidance, quadrotor-payload system, sliding mode control.

I. INTRODUCTION

Unmanned aerial vehicles (UAVs) have been widely used in the civil, military and environmental protection fields in recent years (such as [1], [2], [3], [4], [5], [6]). For example, itfilm and television photography has been involved in cargo transportation [3], film and television photography [4], remote sensing mappingv [5], and precision agriculture [6]. Due to their flexibility and maneuverability, quadrotor UAVs are well-suited to perform load-carrying tasks. Quadrotors usually transport payloads in two ways: robotic arm grasping [7], [8], [9] and cable hanging [11], [12], [13]. The advantage of using a cable for payload transport is that quadrotors do not need to consider the shape of the payload. Meanwhile, the payload neither interferes with the attitude response of the quadrotor nor shifts its barycentric position. It is of great importance to promote the development of UAV technology and research on local obstacle avoidance control of the quadrotor with suspend payload in complex environments.

In terms of modeling, quadrotors are more complex and have the characteristics of multiple degrees of freedom, high coupling, and nonlinearity [14]. Currently, the modeling methods of the quadrotor-payload system are mainly divided into two types: one modeling method is to model the overall dynamics of the quadrotor-payload system and take the

The associate editor coordinating the review of this manuscript and approving it for publication was Xiwang Dong.

suspension load part as the increased degree of freedom, another modeling method is to consider the suspension load part as an external disturbance to the quadrotor system. For example, Guerrero et al. [15] developed an overall dynamical model for the quadrotor-payload system based on the Euler-Lagrange equations, which takes into account the integrated dynamics of the quadrotor and the payload. Yang et al. [16] proposed a complete model of the quadrotor suspended payload system with variable length cable based on the Newton-Euler method, which consists of the motion equations of quadrotor and payload with variable length cable. Moreover, Pizetta et al. [17] modeled the UAV-load system based on Euler-Lagrange equation and regarded the load as a model disturbance in order to simplify the model and controller design.

The swing of the payload will be transmitted to the quadrotor through the cable, making it susceptible to external disturbances and thus affecting the stability of the quadrotor-payload system. Therefore, controller design for the quadrotor-payload system is a problem deserving research [18]. In this respect, common controllers include backstepping control [19], PID control [20], and sliding mode control (SMC) [21]. As far as sliding mode control is concerned, it is robust to disturbances and uncertainties of modeling. Safwat et al. [22] designed robust integral sliding mode controller and robust backstepping sliding mode controller for attitude loop subsystem and position loop subsystem respectively, and verified that the quadrotor can track the reference trajectory under external disturbances. Zhou et al. [23] used PD and SMC to control the quadrotor-payload system, and SMC was shown to have a strong robustness to the disturbances caused by the payload. In this paper, the SMC is used to control the position and attitude of the quadrotor-payload system. In addition, a feed-forward controller is designed to simultaneously suppress payload oscillations.

When the quadrotor suspension payload performs transportation tasks, it should have real-time autonomous obstacle avoidance capability to avoid obstacles exist in the environment [24]. Yang et al. [25] presented a path planning algorithm based on Rapidly-exploring Random Tree (RRT) for UAVs in an unknown and cluttered environment. However, due to the heavy computational load, it is difficult to guarantee fast convergence of the method in practice. In [26], Farid et al. proposed a modified heuristic-based A-star (A*) formalism to avoid extra expanded nodes in 3D path search to generate a dynamically feasible optimal trajectory for quadrotors. The above methods can be viewed as global path planning, which requires global obstacle information and is suitable for tasks with known environments. In addition, in the case of unknown environment, local obstacle avoidance algorithm should be considered. A popular method is employing the artificial potential field (APF), which is used as a superposition of the attractive potential field of the target location and the repulsive potential field of the obstacle to generate an availability path [28]. Montiel et al. [29] proposed a method for UAVs to find optimal paths in static and dynamic environments. Wang et al. [30] proposed an obstacle avoidance method based on improved artificial potential field. Both methods are mainly derived for obstacle avoidance problems and can be viewed as local path planning. Compared to global path planning, it has the advantage that it does not rely on global information and only requires real-time obstacle information detected by the UAV sensors to avoid the nearest obstacle. However, when the APF method is used for local obstacle avoidance of the quadrotor with suspended payload, the obstacle avoidance detection distance of the quadrotor-payload system is usually set to a fixed value, ignoring the problem that the swing of the payload may cause the change of the obstacle avoidance distance of the system [31].

In this paper, to ensure the safe completion of flight missions in environments with dense obstacles and external disturbances, a local obstacle avoidance control scheme for the quadrotor-payload system is designed. Firstly, the overall dynamic model of the quadrotor-payload system, including the dynamics of quadrotor position, attitude, and payload, is established using the Euler-Lagrange equations. Compared to the Newton-Euler modeling method, the modeling process in this paper is relatively simple and accurately describes the motion of the quadrotor. Secondly, in the local obstacle avoidance module, considering that payload swing may cause changes in obstacle avoidance distance, the quadrotor-payload system is obstacle avoidance constrained using the payload's swing angles and the R-function. Then, the traditional APF method is improved to enable the quadrotor to achieve low conservatism in obstacle avoidance detection, approaching and circumventing obstacles as closely as possible while ensuring safety. Thirdly, in the control module, a cascaded sliding mode controller is designed to enhance the robustness of the suspended unmanned aerial vehicle system under external disturbances, and an anti-swing feedforward controller is designed to further suppress payload's swing angles. Finally, the autonomous real-time obstacle avoidance of the quadrotor-payload system is achieved by combining the local obstacle avoidance module and the control module.

The remaining parts of this paper are organized as follows. The quadrotor-payload system model is established in Section II. The improved local obstacle avoidance strategy and the design of the controller are presented in Section III. Section IV carries out the simulation experiment, the comparison simulation results attest to the effectiveness of the proposed scheme. Finally, some conclusions are presented in Section V.

II. MODELE OF THE QUADROTOR-PAYLOAD SYSTEM WITH DISTURBANCES

The schematic of the quadrotor-payload system is shown in Fig. 1. The payload can swing in the 3D space according to its own dynamics, but the swing space is limited by the cable length, which in turn affects the flight performance of the quadrotor. To facilitate the development of a mathematical

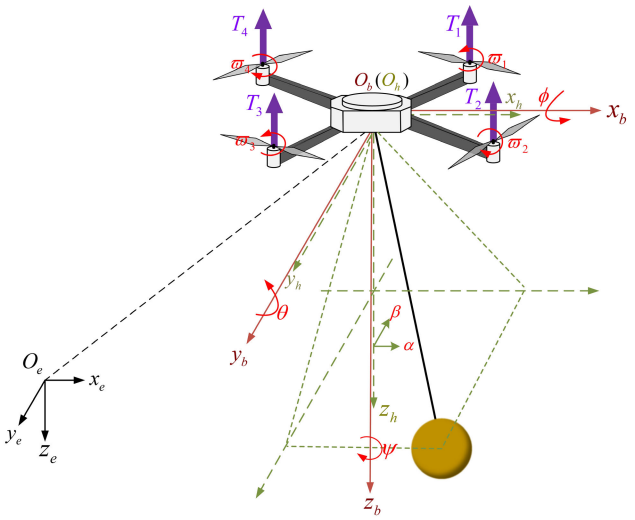

FIGURE 1. Schematic of the quadrotor-payload system (include reference frames, forces and angles).

model of the quadrotor-payload system, the following assumptions are made:

(a) The body of the quadrotor system is rigid and center-symmetric.
(b) The cable attached to the quadrotor is considered rigid and massless.
(c) The payload is considered as a particle, and the swing angles α and β are bounded as follows:

$$-\frac{\pi}{2} < \alpha < \frac{\pi}{2}, \quad -\frac{\pi}{2} < \beta < \frac{\pi}{2}. \tag{1}$$

Before modeling the quadrotor-payload system, it is necessary to establish appropriate coordinate frames. In this case, $\{e\} = \{x_e, y_e, z_e\}$ is the inertial frame, and $\{b\} = \{x_b, y_b, z_b\}$ is the quadrotor body frame whose origin O_b coincides with the center of mass of the quadrotor. In addition, a payload frame $\{h\} = \{x_h, y_h, z_h\}$, whose origin O_h coincides with the origin O_b and orientation is parallel to the inertial frame $\{e\}$ is set up. In frame $\{h\}$, the location of the payload can be obtained. In this article, configure system variables $q = [\,\xi\ \eta\ \mu\,]^T \in \Re^{8\times 1}$, where $\xi = [x\ y\ z]^T$ is the position vector of the quadrotor in the inertial frame $\{e\}$, $\eta = [\phi\ \theta\ \psi]^T$ is the Euler angles vector of the quadrotor which represents roll, pitch and yaw, respectively, and $\mu = [\,\alpha\ \beta\,]^T$ is the swing angle vector of the payload in which α and β are the rotation angles of the payload around the axes y_h and x_h in the payload frame $\{h\}$.

A. PAYLOAD COORDINATE CALCULATION

Let $\xi_p = [x_p\ y_p\ z_p]^T$ denote the position of the payload in the inertial frame $\{e\}$, which is determined by the length of the cable l, the swing angle μ, and the position of the quadrotor ξ. When the payload naturally droops at the initial moment, its position in the frame $\{h\}$ is expressed as

$$\xi_{p_0} = [\,0\ 0\ l\,]^T. \tag{2}$$

When quadrotor moves, the position of the payload is ([27])

$$\xi_p = \xi + T_p \xi_{p_0}, \tag{3}$$

and

$$T_P = Rot(\alpha)Rot(\beta) = \begin{bmatrix} c_\alpha & s_\alpha s_\beta & s_\alpha c_\beta \\ 0 & c_\beta & -s_\beta \\ -s_\alpha & s_\beta c_\alpha & c_\alpha c_\beta \end{bmatrix}, \tag{4}$$

where $c_i = \cos(i)$, $s_i = \sin(i)$, $Rot(\alpha)$ and $Rot(\beta)$ are the rotation matrices around the axes y_h and x_h in the frame $\{h\}$.

B. EULER-LAGRANGE FUNCTION

Then, the dynamic model of the quadrotor-payload system is derived using the Euler-Lagrange method based on the energy principle. The Lagrange function of the quadrotor-payload system is

$$L(q, \dot{q}) = K(q, \dot{q}) - V(q), \tag{5}$$

where

$$\begin{aligned} K(q,\dot{q}) &= K_U + K_P \\ &= (K_{T(uav)} + K_{Rot(uav)}) + (K_{T(load)} + K_{Rot(load)}) \\ &= \left\{ \frac{1}{2} M \dot{\xi}^T \dot{\xi} + \frac{1}{2} \Omega^T I \Omega \right\} \\ &\quad + \left\{ \frac{1}{2} m \dot{\xi}_P^T \dot{\xi}_P + \frac{1}{2} I_p \left(\dot{\alpha}^2 + \dot{\beta}^2 \right) \right\} \end{aligned} \tag{6}$$

is the total kinetic energy which can be expressed as the sum of the kinetic energy K_U of the quadrotor and the kinetic energy K_P of the payload. $K_{T(uav)}$ and $K_{T(load)}$ are the kinetic energy of the quadrotor and payload through translation, and $K_{Rot(uav)}$ and $K_{Rot(load)}$ are the kinetic energy of the quadrotor and payload through rotation, respectively. M and m are the mass of the quadrotor and payload. Ω is the rotation angular velocity matrix of the quadrotor body which is related to $\dot{\eta}$ as follow:

$$\begin{aligned} \Omega &= [\,\omega_{xb} \quad \omega_{yb} \quad \omega_{zb}\,]^T = R_\eta \dot{\eta} \\ &= \begin{bmatrix} 1 & 0 & -s_\theta \\ 0 & c_\phi & s_\phi c_\theta \\ 0 & -s_\phi & c_\phi c_\theta \end{bmatrix} \begin{bmatrix} \dot{\phi} \\ \dot{\theta} \\ \dot{\psi} \end{bmatrix}, \end{aligned} \tag{7}$$

and the moment of inertia matrix of the quadrotor is

$$I = \begin{bmatrix} I_{xx} & I_{xy} & I_{xz} \\ I_{yx} & I_{yy} & I_{yz} \\ I_{zx} & I_{yz} & I_{zz} \end{bmatrix} \tag{8}$$

In (8), I is a symmetric matrix and $I_{xy} = I_{xz} = I_{yz} = 0$ for quadrotors with center symmetry [32]. $I_p \in \Re_+$ is the moment of inertia of the payload. The total potential energy function of the system

$$V(q) = Mg(-z) + mg(-z_p) = Mg(-z) + mg(-z - lc_\alpha c_\beta) \tag{9}$$

results from the sum of the potential energy of the quadrotor and the suspended payload.

Combining (5), (6) and (9), the Lagrangian function can be written as

$$\begin{aligned} L(q,\dot{q}) = & \frac{1}{2}(M+m)\left(\dot{x}^2+\dot{y}^2+\dot{z}^2\right) \\ & + \frac{1}{2}\left(I_{xx}s_\theta^2 + I_{yy}c_\theta^2 s_\phi^2 + I_{zz}c_\theta^2 c_\phi^2\right)\dot{\psi}^2 \\ & + \frac{1}{2}\left(I_{yy}c_\phi^2 + I_{zz}s_\phi^2\right)\dot{\theta}^2 + \frac{1}{2}I_{xx}\dot{\phi}^2 + \frac{1}{2}ml^2\dot{\beta}^2 \\ & - mlc_\beta\dot{y}\dot{\beta} + \frac{1}{2}ml^2\dot{\alpha}^2c_\beta^2 + \frac{1}{2}I_p\left(\dot{\alpha}^2+\dot{\beta}^2\right) \\ & - I_{xx}s_\theta\dot{\psi}\dot{\phi} + \left(I_{yy}-I_{zz}\right)c_\theta c_\phi s_\phi\dot{\psi}\dot{\theta} \\ & - mli\dot{\beta}s_\beta\left(s_\alpha\dot{x}+c_\alpha\dot{z}\right) + mli\dot{\alpha}c_\beta\left(c_\alpha\dot{x}-s_\alpha\dot{z}\right) \\ & + Mgz + mg\left(z + lc_\alpha c_\beta\right) \end{aligned} \tag{10}$$

C. INPUT FORCES AND TORQUES

$T = \sum_{i=1}^{4} c_T\varpi_i{}^2$ is the total pull upward force produced by the quadrotor, and ϖ and c_T are the rotational speed and aerodynamic coefficient of the propeller, respectively.

The vector

$$F = \begin{bmatrix} F_x & F_y & F_z \end{bmatrix}^T = -R_F\begin{bmatrix} 0 & 0 & T \end{bmatrix}^T, \tag{11}$$

represents the component of the forces acting on the axis x_e, y_e, z_e in the frame $\{e\}$ mapped by the rotation of the quadrotor through the attitude angle, and

$$R_F = \begin{bmatrix} c_\theta c_\psi & c_\psi s_\phi s_\theta - c_\phi s_\psi & c_\phi c_\psi s_\theta + s_\phi s_\psi \\ c_\theta s_\psi & s_\phi s_\theta s_\psi + c_\phi c_\psi & c_\phi s_\theta s_\psi - c_\psi s_\phi \\ -s_\theta & s_\phi c_\theta & c_\phi c_\theta \end{bmatrix} \tag{12}$$

is the quadrotor rotation matrix from the frame $\{b\}$ to $\{e\}$.

Evidently, the change of the attitude angle η affects the forward thrust F of the quadrotor, and the torques produced by the propeller is

$$\begin{aligned} \tau &= \begin{bmatrix} \tau_\phi & \tau_\theta & \tau_\psi \end{bmatrix}^T \\ &= \begin{bmatrix} \frac{\sqrt{2}}{2}dc_T & -\frac{\sqrt{2}}{2}dc_T & -\frac{\sqrt{2}}{2}dc_T & \frac{\sqrt{2}}{2}dc_T \\ \frac{\sqrt{2}}{2}dc_T & \frac{\sqrt{2}}{2}dc_T & -\frac{\sqrt{2}}{2}dc_T & -\frac{\sqrt{2}}{2}dc_T \\ c_M & -c_M & c_M & -c_M \end{bmatrix} \\ &\quad \times \begin{bmatrix} \varpi_1^2 \\ \varpi_2^2 \\ \varpi_3^2 \\ \varpi_4^2 \end{bmatrix}, \end{aligned} \tag{13}$$

where d is the distance between the propeller and the center of mass of the quadrotor, c_M is the coefficient of torque.

D. DYNAMICS MODEL OF THE QUADROTOR-PAYLOAD SYSTEM WITH DISTURBANCES

Applying the Euler-Lagrange formulation

$$\frac{d}{dt}\left(\frac{\partial L(q,\dot{q})}{\partial\dot{q}}\right) - \frac{\partial L(q,\dot{q})}{\partial q} = BU + D \tag{14}$$

where $U = \begin{bmatrix} T & \tau_\phi & \tau_\theta & \tau_\psi \end{bmatrix}^T$ is the control input of the system, and

$$B = \begin{bmatrix} -(c_\phi c_\psi s_\theta + s_\phi s_\psi) & 0 & 0 & 0 \\ -(c_\phi s_\theta s_\psi - c_\psi s_\phi) & 0 & 0 & 0 \\ -(c_\phi c_\theta) & 0 & 0 & 0 \\ 0 & 1 & 0 & 0 \\ 0 & 0 & 1 & 0 \\ 0 & 0 & 0 & 1 \\ 0 & 0 & 0 & 0 \\ 0 & 0 & 0 & 0 \end{bmatrix}. \tag{15}$$

Entering (10) into (14), we obtain the equations for the overall dynamics of the quadrotor-payload system, including the position dynamics equation

$$\begin{cases} F_x + d_x = (M+m)\ddot{x} + mlc_\alpha c_\beta\ddot{\alpha} - mls_\alpha s_\beta\ddot{\beta} \\ \qquad -2mls_\beta c_\alpha\dot{\alpha}\dot{\beta} - mlc_\beta s_\alpha\dot{\alpha}^2 - mlc_\beta s_\alpha\dot{\beta}^2 \\ F_y + d_y = (M+m)\ddot{y} - mlc_\beta\ddot{\beta} + mls_\beta\dot{\beta}^2 \\ F_z + d_z = (M+m)\ddot{z} - mls_\alpha c_\beta\ddot{\alpha} - mlc_\alpha s_\beta\ddot{\beta} + 2mls_\beta s_\alpha\dot{\alpha}\dot{\beta} \\ \qquad -mlc_\beta c_\alpha\dot{\alpha}^2 - mlc_\beta c_\alpha\dot{\beta}^2 - (M+m)g \end{cases} \tag{16}$$

the attitude dynamics equation

$$\begin{cases} \tau_\phi + d_\phi = I_{xx}\ddot{\phi} - I_{xx}s_\theta\ddot{\psi} - \left(I_{yy}-I_{zz}\right)s_\phi c_\phi c_\theta^2\dot{\psi}^2 \\ \quad + \left\{-I_{xx}\dot{\psi}c_\theta + \left(I_{yy}-I_{zz}\right)\left(\dot{\theta}s_\phi c_\phi + \dot{\psi}c_\theta s_\phi^2 - \dot{\psi}c_\theta c_\phi^2\right)\right\}\dot{\theta}; \\ \tau_\theta + d_\phi = \left\{I_{yy}c_\phi^2 + I_{zz}s_\phi^2\right\}\ddot{\theta} + \left\{\left(I_{yy}-I_{zz}\right)c_\theta c_\phi s_\phi\right\}\ddot{\psi} \\ \quad + \left\{I_{xx}\dot{\psi}c_\theta + \left(I_{yy}-I_{zz}\right)\left(-2\dot{\theta}s_\phi c_\phi + \dot{\psi}c_\theta c_\phi^2 - \dot{\psi}c_\theta s_\phi^2\right)\right\}\dot{\phi} \\ \quad + s_\theta c_\theta\left(-I_{xx} + I_{yy}s_\phi^2 + I_{zz}c_\phi^2\right)\dot{\psi}^2; \\ \tau_\psi + d_\psi = -I_{xx}s_\theta\ddot{\phi} + \left(I_{yy}-I_{zz}\right)c_\theta c_\phi s_\phi\ddot{\theta} \\ \quad + \left\{I_{xx}s_\theta^2 + c_\theta^2\left(I_{zz}c_\phi^2 + I_{yy}s_\phi^2\right)\right\}\ddot{\psi} - I_{zz}\dot{\phi}c_\theta^2 s_\phi c_\phi\dot{\psi} \\ \quad - \left\{I_{xx}\dot{\theta}c_\theta - \left(I_{yy}-I_{zz}\right)\dot{\psi}c_\theta^2 s_\phi c_\phi\right\}\dot{\phi} + I_{yy}\dot{\phi}c_\theta^2 s_\phi c_\phi\dot{\psi} \\ \quad + \left\{I_{xx}\dot{\psi}s_\theta c_\theta - \left(I_{yy}-I_{zz}\right)\left(\dot{\theta}s_\theta c_\phi s_\phi + \dot{\phi}c_\theta s_\phi^2 - \dot{\phi}c_\theta c_\phi^2\right)\right\}\dot{\theta} \\ \quad + \left\{I_{xx}\dot{\theta}s_\theta c_\theta - 2\left(I_{yy}s_\phi^2 + I_{zz}c_\phi^2\right)\dot{\theta}s_\theta c_\theta\right\}\dot{\psi}; \end{cases} \tag{17}$$

and the dynamic equation of payload's swing angles

$$\begin{cases} \ddot{\alpha} = \dfrac{(-c_\alpha c_\beta\ddot{x} + s_\alpha c_\beta\ddot{z} + 2li\dot{\alpha}\dot{\beta}c_\beta s_\beta - gc_\beta s_\alpha)ml}{(I_p + ml^2c_\beta^2)} \\ \ddot{\beta} = \dfrac{(s_\alpha s_\beta\ddot{x} + c_\beta\ddot{y} + c_\alpha s_\beta\ddot{z} + li\dot{\alpha}^2c_\beta s_\beta + gs_\beta c_\alpha)ml}{(I_p + ml^2)} \end{cases} \tag{18}$$

in which $D = \begin{bmatrix} d_x & d_y & d_z & d_\phi & d_\theta & d_\psi & 0 & 0 \end{bmatrix}^T$ is the vector of external disturbances.

Equations (11) – (13) and (16) – (18) constitute the mathematical model of the quadrotor-payload system with external disturbances, and the matrix form can be abbreviated as

$$M(q)\ddot{q} + C(q,\dot{q})\dot{q} + G(q) = BU + D, \tag{19}$$

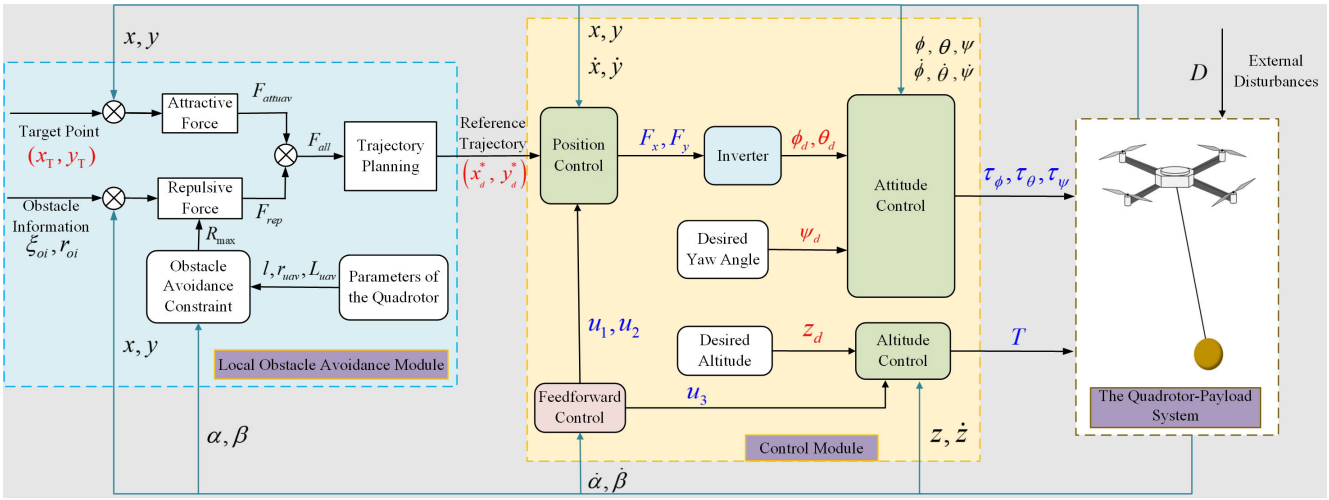

FIGURE 2. Scheme of local obstacle avoidance and trajectory tracking control.

where $M(q)$ is the inertia matrix, $C(q, \dot{q})$ is the Coriolis and centrifugal matrix, and $G(q)$ is the gravitational vector ([17]). From the modeling analysis, it can be seen that the swing of the payload will affect the motion state of the quadrotor, which can be clearly illustrated by (16) and (18).

III. LOCAL OBSTACLE AVOIDANCE AND TRAJECTORY TRACKING CONTROL

This section describes the design of local obstacle avoidance module and control module, respectively (Fig. 2). In the local obstacle avoidance module, a R-function is used to describe the quadrotor-payload system to obtain the maximum envelope radius. Then the traditional APF is improved to obtain the feasible desired path. In the control module, a position controller and an attitude controller with strong anti-interference, as well as a feed-forward controller are designed to suppress the swing angles.

A. LOCAL OBSTACLE AVOIDANCE MODULE DESIGN

The local obstacle avoidance module is designed to bypass obstacles to obtain a safe flight path. The input information of this module is the location of the target point $\xi_T = (x_T \ y_T)$, obstacle information, quadrotors related parameters, the real flight trajectory $\xi^* = (x \ y)$, and the swing angles α and β of the payload. The output is the reference trajectory $\xi_d{}^* = (x_d^* \ y_d^*)$. The remainder of this part introduces obstacle avoidance constraint, the traditional APF and the improved APF, respectively.

1) OBSTACLE AVOIDANCE CONSTRAINT

Assuming the quadrotor flies at a predetermined altitude in an environment with multiple vertical obstacles, only the shape of the quadrotor-payload system should be depicted in the X-Y plane. Moreover, considering the swing of the payload, the position of the payload ξ_p is considered when the quadrotor performs obstacle avoidance.

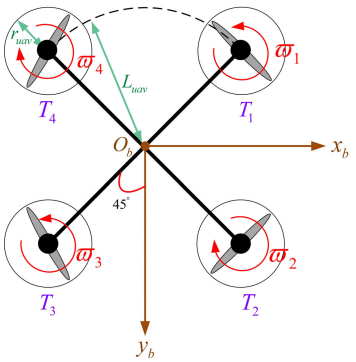

(a) 'X' shaped of the quadrotor plane diagram.

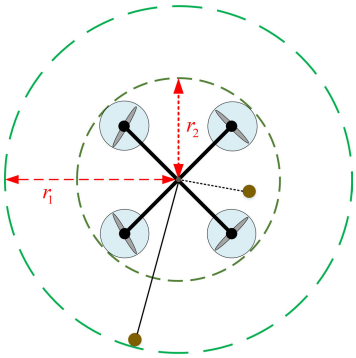

(b) Two possible envelope circular radii.

FIGURE 3. The obstacle avoidance constraint diagram of the quadrotor-payload system.

The obstacle avoidance constraint diagram of the quadrotor-payload system is shown in Fig. 3. To enable the quadrotor to safely fly around obstacles, we consider the problem of collision avoidance envelope circle switching caused by the swing of the payload. When the payload position exceeds the envelope range of the quadrotors body,

the overall envelope radius of the system is r_1; When the payload position does not exceed the envelope range of the quadrotors body, the overall envelope radius is r_2, as follows

$$\begin{cases} r_1 = \sqrt{l^2\left(w_1^2 + w_2^2\right)} \\ r_2 = r_{uav} + L_{uav}, \end{cases} \tag{20}$$

where $w_1 = c_\beta s_\alpha$, $w_2 = s_\beta$, r_{uav} and L_{uav} represent the arm length and propeller radius of the quadrotor, respectively.

To better describe the shape of the quadrotor-payload system, the maximum envelope circular radius of the quadrotor-payload system model can be obtained based on the mathematical idea of the R-function as follows [31], [33]. Combining (3) and (20) yields the maximum envelope circular radius

$$R_{\max} = \frac{1}{2}\left(r_1 + r_2 + |r_1 - r_2|\right) \tag{21}$$

Obviously, when performing collision detection, we abstract the system into an envelope circle of radius $R_{\max}$, which is more in line with the actual situation of quadrotor flight. Moreover, considering the possible bias in the quadrotor localization accuracy, an appropriate safety distance $\Delta d_{\min}$ can be added to enable the system to safely avoid vertical obstacles.

2) TRADITIONAL APF

The artificial potential field method was proposed by Khatib in the 1980s [28]. The basic idea of traditional APF is to design the unknown environment in which the robot moves as a virtual force field. It assumes that the target point and the obstacle generates an attractive force field and a repulsive force field to the robot, respectively. The robot eventually generates a safe obstacle avoidance path from the starting position to the target position under the traction of the attractive and repulsive forces in the virtual potential field. The traditional APF algorithm can be expressed as follows:

$$U_{attuav} = \frac{1}{2}k_a[\rho(\xi_T, \xi^*)]^2, \tag{22}$$

$$F_{attuav} = -grad\left[U_{attuav}\right] = k_a\rho(\xi_T, \xi^*)\nabla\rho(\xi_T, \xi^*), \tag{23}$$

$$U_{repuavi} = \begin{cases} \frac{1}{2}k_{ri}[\frac{1}{\rho_{oi}(\xi^*, \xi_{oi})} - \frac{1}{\rho_0}]^2, & \rho_{oi} \le \rho_0; \\ 0, & \rho_{oi} > \rho_0. \end{cases} \tag{24}$$

$$F_{repuavi} = -grad\left[U_{repuavi}\right] = \begin{cases} k_{ri}[\frac{1}{\rho_{oi}(\xi^*, \xi_{oi})} - \frac{1}{\rho_0}]\frac{1}{\rho_{oi}{}^2(\xi^*, \xi_{oi})}\nabla\rho_{oi}(\xi^*, \xi_{oi}), \\ \qquad \rho_{oi} \le \rho_0; \\ 0, \\ \qquad \rho_{oi} > \rho_0 \end{cases} \tag{25}$$

$$F_{alluav} = F_{attuav} + \sum_{i=1}^{n} F_{repuavi} \tag{26}$$

Among them, U_{attuav} and $U_{repuavi}$ are the target attraction potential field function and the i-th obstacle repulsion potential field function, respectively; F_{attuav} and $F_{repuavi}$ are the attractive force and the i-th repulsive force, respectively; F_{alluav} is the resultant force. $\rho_{oi}(\xi^*, \xi_{oi})$ is the actual distance between the i-th obstacle and the robot, $\rho(\xi_T, \xi^*)$ is the actual distance between the target point and the robot, ρ_0 is the safe distance between the robot and the obstacle; $\nabla\rho(\xi_T, \xi^*)$ and $\nabla\rho_{oi}(\xi^*, \xi_{oi})$ are denoted as unit vectors from ξ^* to ξ_T and from ξ_{oi} to ξ^*, respectively. k_a and k_{ri} are the attraction and repulsion coefficients, respectively.

When performing local obstacle avoidance, APF does not need to know all obstacle information, it only works within the influence range of the nearest obstacle, and it is highly adaptable to unknown environments. Therefore, the APF method is well-suited to solve the real-time obstacle avoidance problem of quadrotors in unknown environments.

3) IMPROVED APF FOR QUADROTOR-PAYLOAD SYSTEM

The traditional APF method has many advantages as a local obstacle avoidance method, but when it is applied to the obstacle avoidance of the quadrotor-payload system, if the obstacle avoidance distance is directly defined as the cable length (l), although the flight of the quadr is safer, it will cause a waste of space. If only the radius of the quadrotor body is considered, it cannot be used when the payload exceeds the body, in which case there may be a risk of collision with obstacles. Next, R_{max} is used to constrain the envelope of the quadrotor-payload system and thus achieve less conservative obstacle avoidance. Considering the real-time swing position of the payload, the improved repulsive force function is designed as follows:

$$F_{repi} = \begin{cases} k_{ri}[\frac{1}{\rho_{oi}(\xi^*, \xi_{oi})} - \frac{1}{\rho^*}]\frac{1}{\rho_{oi}{}^2(\xi^*, \xi_{oi})}\nabla\rho_{oi}(\xi^*, \xi_{oi}), \\ \qquad \rho_{oi} - \rho^* \le 0; \\ 0, \\ \qquad \rho_{oi} - \rho^* > 0; \end{cases}$$

$$\rho^* = R_{\max} + r_{oi} + \Delta d_{\min} \tag{27}$$

$$F_{all} = F_{attuav} + \sum_{i=1}^{n} F_{repi} \tag{28}$$

where r_{oi} is the radius of the i-th obstacle and R_{max} is the maximum envelope circular radius of the quadrotor-payload system.

Remark 1: The virtual force diagram of the improved APF is shown in Fig. 4. The envelope circular is used for obstacle avoidance constraints of the quadrotor-payload system. Obviously, changing the original obstacle avoidance distance ρ_0 ($\rho_0 = l + r_{oi} + \Delta d_{\min}$) to ρ_0^* ($\rho_0^* = R_{\max} + r_{oi} + \Delta d_{\min}$) with the change of the swing angle can achieve less conservative obstacle avoidance detection. The application of the improved APF function for obstacle avoidance is closer to the practical case of quadrotor-payload flight, which has the advantage of improving the timeliness and safety of flying.

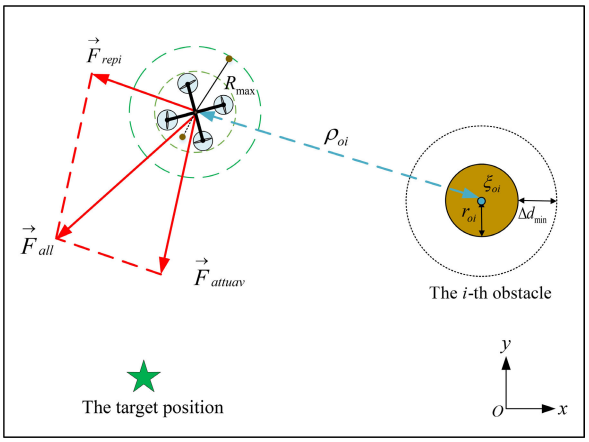

FIGURE 4. Schematic of the virtual force of the improved APF.

Furthermore, the desired trajectory $\xi_d{}^* = (x_d^* \; y_d^*)$ of the quadrotor can be obtained by using the force F_{all}.

As an effective obstacle avoidance method, the traditional APF method has many advantages. However, in some cases, the traditional APF may encounter the problem of getting trapped in a local optimum [34], [35], [36]. Since the main work of this paper is to verify the effectiveness of the real-time obstacle avoidance method using the improved APF for the quadrotor-payload system, we will not consider the scenario where the UAV falls into a local optimum for the time being.

B. CONTROL MODULE DESIGN

A cascade control scheme (Fig.2) based on sliding mode algorithm is designed for the quadrotor-payload system trajectory tracking under wind disturbances, which includes position controller and attitude controller. The cascade controller is to ensure the quadrotor track the desired trajectory (x_d^*, y_d^*, z_d) asymptotically. Meanwhile, F_x and F_y are virtual control inputs obtained by the position controller, which can be used to derive the desired references of roll angle ϕ_d and pitch angle θ_d. T and $\tau_\phi \sim \tau_\psi$ are used to control the altitude and attitude of the quadrotor-payload system. Moreover, considering the possible swing of the payload, a feedforward controller is designed.

1) POSITION CONTROLLER DESIGN

From (16), the position dynamics model of the quadrotor-payload system can be written as:

$$\begin{cases} (M+m)\ddot{x} = F_x + f_1 + d_x \\ (M+m)\ddot{y} = F_y + f_2 + d_y \\ (M+m)\ddot{z} = F_z + f_3 + (M+m)g + d_z, \end{cases} \tag{29}$$

where $f_1 = -mlc_\alpha c_\beta \ddot{\alpha} + ms_\alpha s_\beta l\ddot{\beta} + ml(\dot{\beta}s_\beta c_\alpha + c_\beta s_\alpha \dot{\alpha})\dot{\alpha} + ml(\dot{\beta}c_\beta s_\alpha + \dot{\alpha}s_\beta c_\alpha)\dot{\beta}$; $f_2 = mlc_\beta \ddot{\beta} - mls_\beta \dot{\beta}^2$; $f_3 = mls_\alpha c_\beta \ddot{\alpha} + mlc_\alpha s_\beta \ddot{\beta} - ml(\dot{\beta}s_\beta s_\alpha - \dot{\alpha}c_\beta c_\alpha)\dot{\alpha} - ml(\dot{\alpha}s_\beta s_\alpha - \dot{\beta}c_\beta c_\alpha)\dot{\beta}$, $f_1 \sim f_3$ can be viewed as the influences the payload exerts on the quadrotor. $d_x \sim d_z$ are the external wind disturbances,which are bounded ($|d_\xi(t)| \le \lambda_\xi$), λ_ξ is a positive real number.

Firstly, define quadrotor reference position $\xi_r = [x_d^* \; y_d^* \; z_d]^T$ and the actual position $\xi = [x \; y \; z]^T$, then the position tracking error and derivative are given as follows:

$$e_\xi = \xi_r - \xi, \dot{e}_\xi = \dot{\xi}_r - \dot{\xi}. \tag{30}$$

Take the design of x-direction position controller as an example, the sliding mode error surface of the position is

$$S_x = c_1 e_x + \dot{e}_x, \tag{31}$$

where c_1 is a positive number.

The control inputs F_x for the x-direction position is designed as

$$F_x = (M+m)(c_1\dot{e}_x + \ddot{x}_d^* + k_1 S_x) - f_1 + k_x sat(S_x), \tag{32}$$

and

$$sat(S_x) = \begin{cases} 1 & S_x > \Delta \\ \gamma S_x & |S_x| \le \Delta \\ -1 & S_x < -\Delta \end{cases}, \quad \gamma = \frac{1}{\Delta}$$

where k_1 and k_x are control parameters which are positive constants.

Select the Lyapunov function L_1 as

$$L_1 = \frac{1}{2}S_x^2, \tag{33}$$

the time derivative of L_1 is

$$\dot{L}_1 = S_x\dot{S}_x = S_x\left\{c_1(\dot{x}_d^* - \dot{x}) - \frac{F_x + f_1 + d_x}{M+m} + \ddot{x}_d^*\right\}. \tag{34}$$

Entering control laws (32) into (34),

$$\dot{L}_1 = -k_1 S_x^2 + \frac{-S_x d_x - k_x S_x sat(S_x)}{M+m}. \tag{35}$$

Adjust the parameters $k_x \ge \lambda_x$,

$$\dot{L}_1 \le -k_1 S_x^2 \le 0. \tag{36}$$

Then, the x-direction position is asymptotically stable.

Similar to (32), the position controller in the y and z directions position are designed as follows:

$$\begin{cases} F_y = (M+m)(c_y\dot{e}_y + \ddot{y}_d^* + k_2 S_y) - f_2 + k_y sat(S_y) \\ F_z = (M+m)(c_z\dot{e}_z + \ddot{z}_d + k_3 S_z - g) - f_3 + k_z sat(S_z), \end{cases} \tag{37}$$

where k_2, k_3, k_y, k_z are all positive numbers, and $k_y \ge \lambda_y$, $k_z \ge \lambda_z$.

Finally, the desired attitude ϕ_d , θ_d and upward force T can be solved as ([16])

$$\begin{cases} \psi_d = command value \\ \phi_d = \arctan\left(\dfrac{(F_x s_{\psi_d} - F_y c_{\psi_d})c_{\theta_d}}{F_z}\right) \\ \theta_d = \arctan\left(\dfrac{F_x c_{\psi_d} + F_y s_{\psi_d}}{F_z}\right) \\ T = \left(\dfrac{F_z}{c_{\phi_d} s_{\theta_d}}\right). \end{cases} \tag{38}$$

2) ATTITUDE CONTROLLER DESIGN

Attitude control of the quadrotor is the crucial part for stabilization and tracking. From (17), the attitude dynamics model of the quadrotor-payload system can be written as

$$\begin{cases} \ddot{\phi} = f_4 + g_1\tau_\phi + g_1 d_\phi \\ \ddot{\theta} = f_5 + g_2\tau_\theta + g_2 d_\theta \\ \ddot{\psi} = f_6 + g_3\tau_\psi + g_3 d_\psi, \end{cases} \tag{39}$$

where f_4 to f_6 are known functions by (17), $g_1 = 1/I_{xx}$, $g_2 = 1/(I_{yy}c_\phi^2 + I_{zz}s_\phi^2)$, $g_3 = 1/\{I_{xx}s_\theta^2 + c_\theta^2(I_{zz}c_\phi^2 + I_{yy}s_\phi^2)\}$; d_ϕ to d_ψ is the external wind disturbance vector,which is bounded ($\left|d_\eta(t)\right| \leq \lambda_\eta$), λ_η is a positive real number.

The desired attitude Angle $\eta_r = [\,\phi_d \;\; \theta_d \;\; \theta_d\,]^T$ is obtained by the position controller. The attitude tracking error of the quadrotor and its derivatives are given as

$$e_\eta = \eta_r - \eta\,,\; \dot{e}_\eta = \dot{\eta}_r - \dot{\eta}. \tag{40}$$

Take the design of roll angle ϕ controller as an example, the sliding mode error surface of the attitude angle is

$$S_\phi = c_\phi e_\phi + \dot{e}_\phi, \tag{41}$$

where c_ϕ is a positive number.

The control inputs τ_ϕ for the roll angle is designed as

$$\tau_\phi = [c_\phi \dot{e}_\phi + \ddot{\phi}_d + k_4 S_\phi - f_4]/g_1 + k_\phi sat(S_\phi) \tag{42}$$

Select the Lyapunov function L_2 as

$$L_2 = \frac{1}{2}S_\phi^2, \tag{43}$$

the time derivative of L_2 is

$$\dot{L}_2 = S_\phi \dot{S}_\phi = S_\phi \left\{c_\phi \dot{e}_\phi + \ddot{\phi}_d - f_4 - g_1\tau_\phi - g_1 d_\phi\right\}. \tag{44}$$

Entering control laws (42) into (44),

$$\dot{L}_2 = -k_4 S_\phi^2 + \left\{-S_\phi d_\phi - k_\phi S_\phi sat(S_\phi)\right\} g_1 \tag{45}$$

Adjust the parameters $k_\phi \geq \lambda_\phi$,

$$\dot{L}_2 \leq -k_4 S_\phi^2 \leq 0. \tag{46}$$

Then, the roll angle is asymptotically stable.

Similar to (42), the attitude controller in the θ and ψ angles are designed as follows:

$$\begin{cases} \tau_\theta = [c_\theta \dot{e}_\theta + \ddot{\theta}_d + k_5 S_\phi - f_5]/g_2 + k_\theta sat(S_\phi) \\ \tau_\psi = [c_\psi \dot{e}_\psi + \ddot{\psi}_d + k_6 S_\psi - f_6]/g_3 + k_\psi sat(S_\psi), \end{cases} \tag{47}$$

where $k_5, k_6, k_\theta, k_\psi$ are all positive numbers, and $k_\theta \geq \lambda_\theta$, $k_\psi \geq \lambda_\psi$.

3) FEED-FORWARD CONTROLLER DESIGN

When the quadrotor is carrying a payload for flight, severe oscillations of the payload's swing angles can affect the stability of the quadrotor-payload system. According to Equation (18), the dynamic of the swing angles α and β have a direct relationship with the position acceleration of the quadrotor. The feed-forward controller are designed as follows:

$$\begin{cases} u_1 = a_1\dot{\alpha} \\ u_2 = a_2\dot{\beta} \\ u_3 = a_1\dot{\alpha} + a_2\dot{\beta}, \end{cases} \tag{48}$$

where a_1 and a_2 are control parameters which are positive constants. Combining the feedforward controller (48) with the control scheme designed in this paper, the quadrotor can not only achieve accurate trajectory tracking, but also restrain the payload's swing.

TABLE 1. Parameters of the quadrotor [16].

Parameter	Value	Units
M	1.25	kg
m	0.25	kg
g	9.81	$\mathrm{m/s^2}$
I_{xx}	0.0087	$\mathrm{kg \cdot m^2}$
I_{yy}	0.0087	$\mathrm{kg \cdot m^2}$
I_{zz}	0.016	$\mathrm{kg \cdot m^2}$
I_p	1.00e-6	$\mathrm{kg \cdot m^2}$
l	1.00	m
r_{uav}	0.10	m
L_{uav}	0.18	m

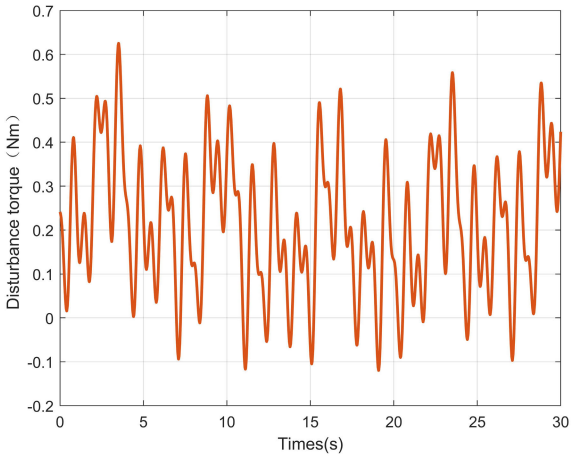

FIGURE 5. The wind disturbances in simulation.

IV. SIMULATION

Simulation experiments are carried out in MATLAB/SIMULINK to verify the effectiveness of the improved local obstacle avoidance algorithm and the proposed control scheme. The parameters of the quadrotor-payload system used in the simulation are shown in Table 1. (As the direction of the gravity is specified to be the positive direction of the z-axis when modeling, the payload coordinates are mapped below the quadrotor in the simulation for easy observation.)

Simulation experiments are mainly carried out in two groups. In group 1, the quadrotor with the suspension payload flies in an obstacle-free environment and we compare cascade sliding mode control algorithm designed in this paper

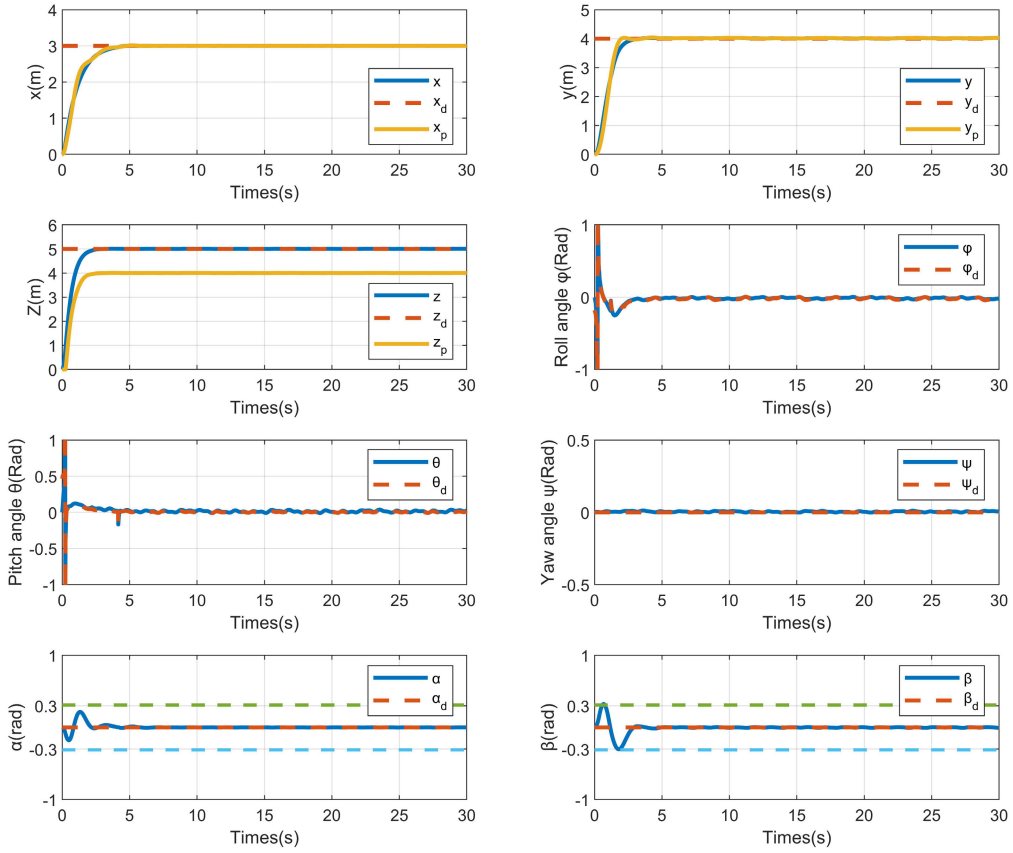

FIGURE 6. Simulation results: cascade sliding mode control with feed-forward.

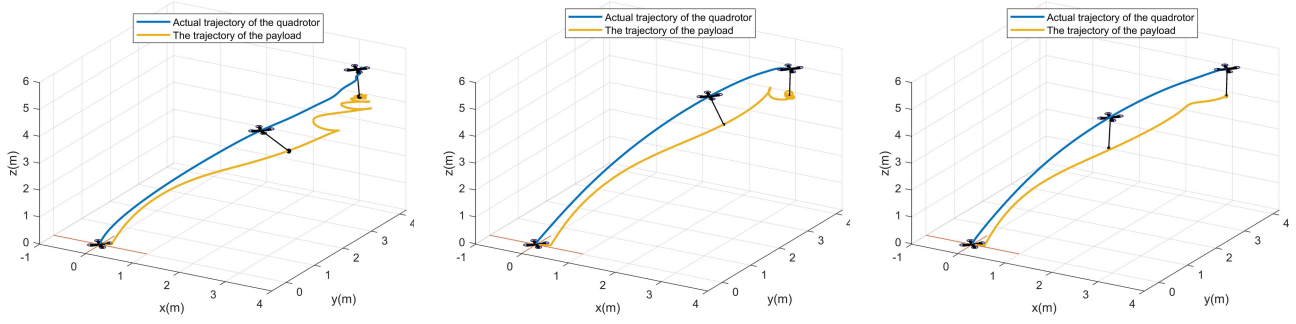

FIGURE 7. The 3D trajectory diagram of the quadrotor carrying payload. [Fig. 7(a) Traditional cascade PID control without feed-forward; Fig. 7(b) Cascade sliding mode control without feed-forward; Fig. 7(c) Cascade sliding mode control with feed-forward.]

TABLE 2. Obstacle information.

obstacle	x-axis (m)	y-axis (m)	height (m)	radius of the i-th obstacle r_{oi} (m)	safe distance $\Delta d_{\min}$ (m)
obs1	3.00	-0.22	4.00	0.30	0.10
obs2	6.00	0.50	4.00	0.20	0.10
obs3	5.00	1.20	4.00	0.30	0.10
obs4	4.00	-1.00	4.00	0.30	0.10
obs5	8.00	-0.40	4.00	0.30	0.10

with the traditional PID control algorithm, followed by the feed-forward controller added to verify the suppression effect on the payload's swing angles. In group 2, the quadrotor with suspension payload flies in an environment crowded of obstacles, and the improved APF in this paper is compared with the traditional APF to verify the performance of the

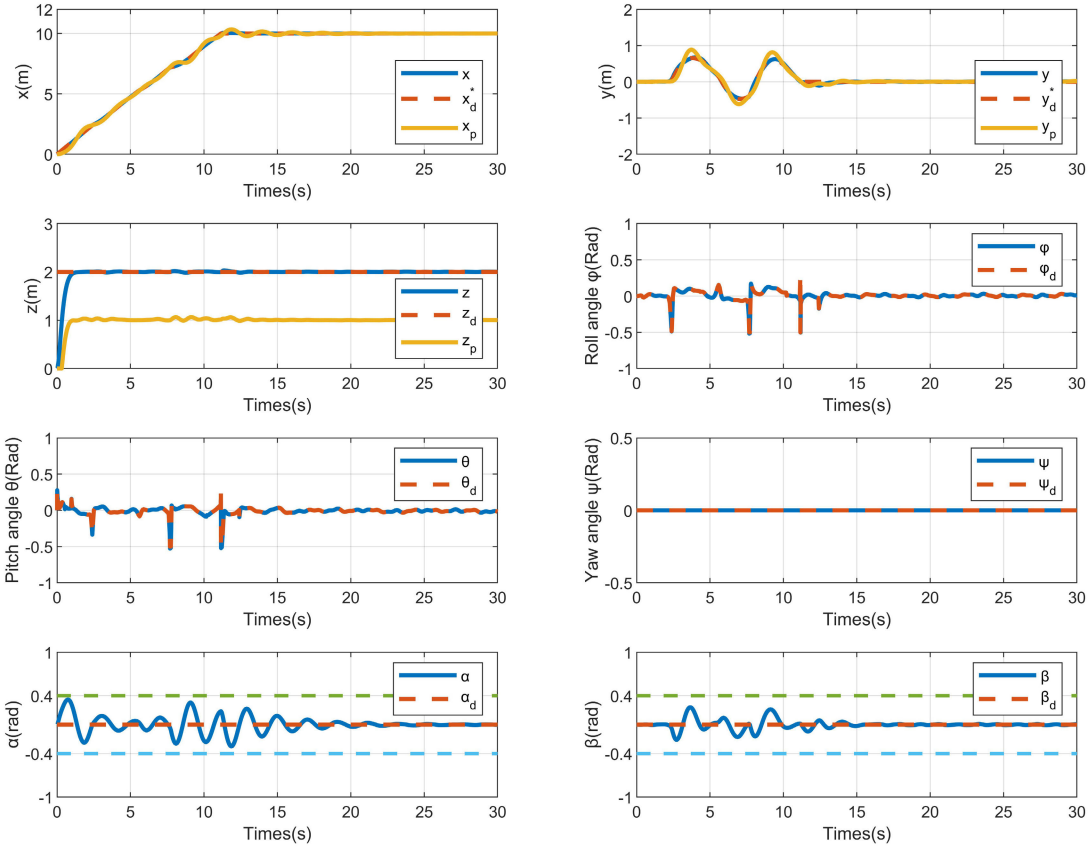

FIGURE 8. Simulation results: tracking based on the traditional APF method.

local real-time obstacle avoidance. Meanwhile, an external wind disturbances always exist during the simulation. The disturbance torques generated by the wind field used in the numerical simulations are as follow [37]:

$$\begin{aligned} d_x = d_y = d_z = d_\phi = d_\theta = d_\psi \\ = 0.14\sin(1.5\pi t - 3.0) - 0.05\sin(2.0\pi t + 7.0) \\ + 0.08\sin(0.6\pi t - 4.0) + 0.09\sin(0.3\pi t + 5.0) \\ - 0.10\sin(3.0\pi t + 3.5) + 0.23 \end{aligned} \tag{49}$$

which is shown in Fig. 5.

A. GROUP 1: PAYLOAD TRANSPORTATION IN AN ENVIRONMENT WITHOUT OBSTACLES

The quadrotor UAV carries the payload and takes off from the origin to the target position $\xi_d = (3\ 4\ 5)$. There are no obstacles during the flight, and the participation of the obstacle avoidance module is not needed. The simulation results of cascade sliding mode control with feed-forward are shown in Fig. 6. The swing angles α and β are all within 0.3 rad and the swing angles of the payload tends to be zero after 5s. The 3D trajectories of the three schemes are shown in Fig. 7.

Through comparing the simulation results in Fig. 6, the proposed method has better performance in position control, attitude control, and suppressed the payload swing angles. Furthermore, from Fig. 7, it is clear that 3D trajectories of the quadrotor and payload under the proposed control scheme are smoother, and the payload's swing angles are smaller than that of cascaded PID control scheme. Moreover, the addition of feed-forward controller can further reduce the payload swing, as well as the sliding mode controller can effectively improve the robustness of the system against wind disturbance.

B. GROUP 2: NAVIGATING IN AN ENVIRONMENT CROWDED OF OBSTACLES

The simulation of autonomous local trajectory planning and multi-obastacle avoidance for quadrotor payload system is developed. The specific environment we are considering is a forest, characterized by multiple vertical obstacles (tree trunks with canopies) and wind interference. The tree canopy is dense, making it impossible for UAVs to fly directly over it. In order to accomplish the rescue mission, the UAV will fly below the tree canopy and carry the payload through a cable to the location of the injured person (coordinates $\xi_d = (10\ 0\ 2)$ known through the GPS) to complete the rescue mission. The quadrotor will maintain a fixed altitude below the tree canopy during its flight, which will prevent collisions with ground vegetation and other obstacles, and the

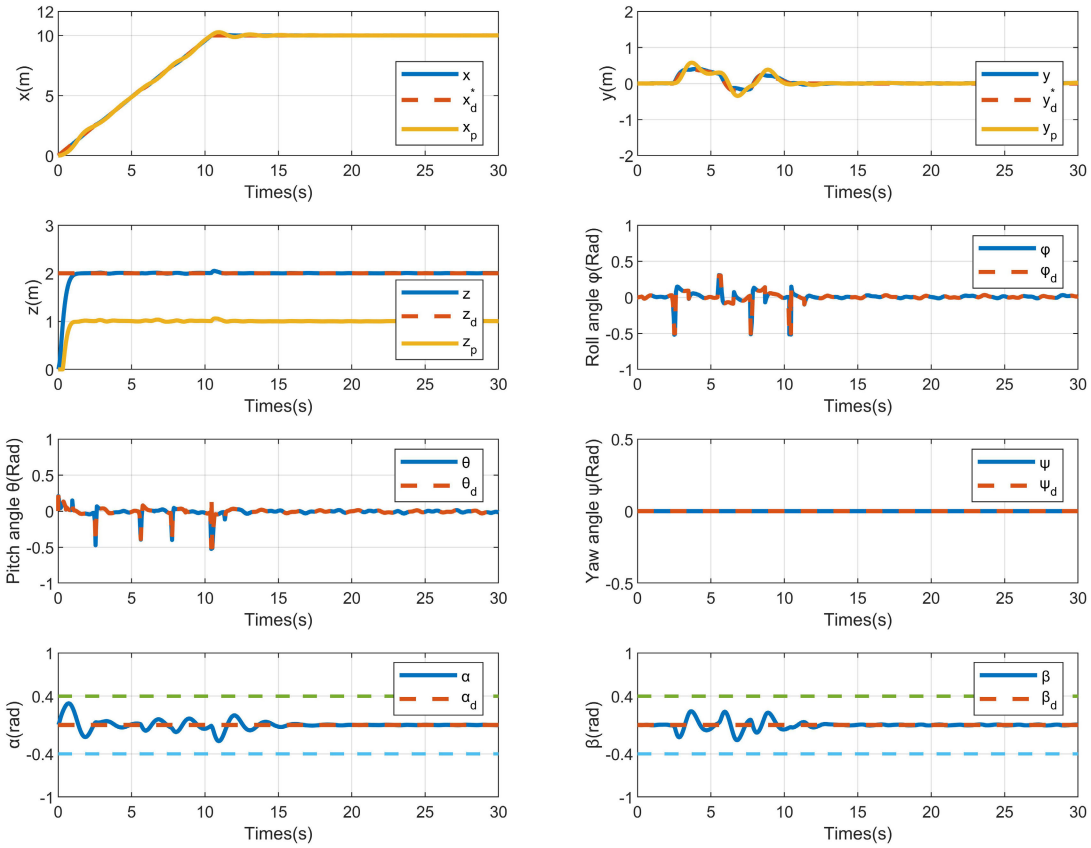

FIGURE 9. Simulation results: tracking based on the improved APF method.

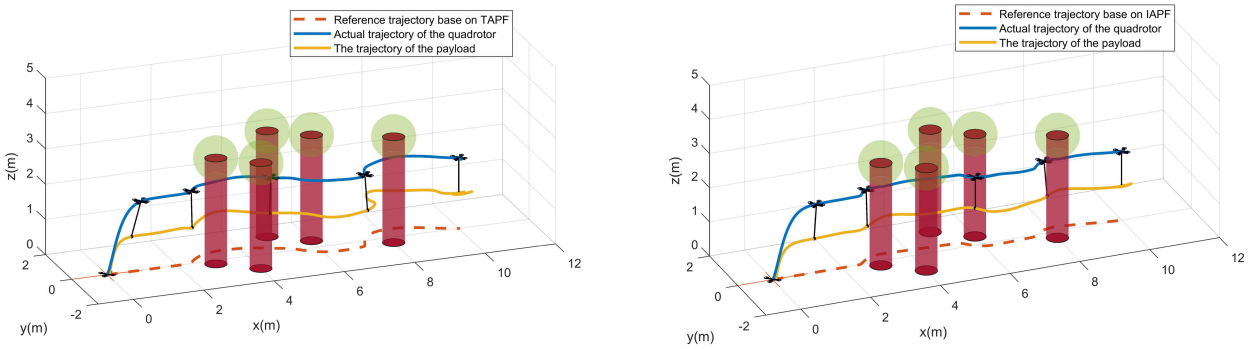

(a) Tracking under traditional APF. (b) Tracking under improved APF.

FIGURE 10. The 3D trajectory diagram of the quadrotor carrying payload for real-time obstacle avoidance.

main obstacles in the navigation environment are the vertical obstacles (tree trunks), and an external wind interferences are always present in the flight environment. Meanwhile, five obstacles are established in the simulated environment and obstacle information is shown in Table 2. The cascade sliding mode control scheme with feed-forward is adopted.

The simulation results of local real-time obstacle avoidance based on the traditional APF are shown in Fig. 8. We observe that the payload's swing angles (α and β) amplitude of the payload are within 0.4 rad, and the swing angles tend to be zero after 20s. It takes about 13s for the quadrotor to reach the target position. The simulation results of the local real-time obstacle avoidance based on the improved APF are shown in Fig. 9. The swing angles (α and β) of the payload are within 0.3 rad and tend to be zero after 15s. Moreover, the quadrotor needs about 10s to reach the target position.

The 3D trajectory diagram and 2D plane diagram of the quadrotor with suspended payload for real-time obstacle avoidance are shown in Fig. 10, Fig. 11

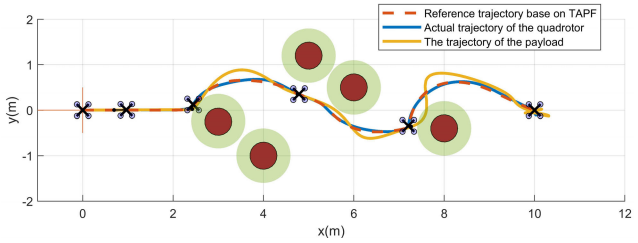

FIGURE 11. The 2D plane diagram of the quadrotor carrying payload for real-time obstacle avoidance based on the traditional APF method. [The green shade indicates the tree crown.]

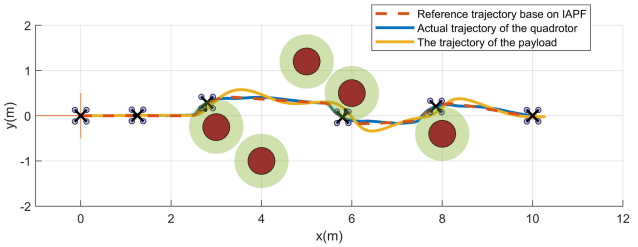

FIGURE 12. The 2D plane diagram of the quadrotor carrying payload for real-time obstacle avoidance based on the improved APF method. [The green shade indicates the tree crown.]

and Fig. 12, respectively. As can be seen from Fig. 10, the improved obstacle avoidance path is shorter than the traditional path, enabling the quadrotor using a smaller turning radius and thus saving space resources. Furthermore, comparing Fig. 11 with Fig. 12 shows that the improved obstacle avoidance strategy enables the quadrotor-payload system to achieve obstacle avoidance with a lower degree of conservatism, which enables the quadrotor to fly as close to and around obstacles as possible while ensuring safety. At the same time, it is clear that the trajectory of the payload is smoother.

Through the above experimental analysis, it can be seen that the combination of the improved APF and the control scheme makes the movement trajectory of the quadrotor shorter and more efficient, as well as can ensure real-time obstacle avoidance and trajectory tracking at small range. At the same time, the quadrotor can reach the target position in a faster time, which improves the timeliness of the rescue. Furthermore, the shortening of the path and the reduction of the swing angles of the payload save the space utilization rate of the quadrotor-payload system and somewhat reduces the occurrence of unexpected situations in the field environment.

V. CONCLUSION

This paper presents a local obstacle avoidance control scheme for the quadrotor with suspended payload, which is suitable for complex environments with dense obstacles and external disturbances. Firstly, the overall dynamic model of the quadrotor-payload system is established by Euler-Lagrange equations, which contains the dynamics of the quadrotor and payload. Secondly, to address the issue of envelope circle radius switching caused by changes in the amplitude of the payload's swing angles, an obstacle avoidance constraint for the quadrotor-payload system is proposed. This constraint incorporates an R-function to enhance the traditional Artificial Potential Field method. The improved APF approach achieves less conservative obstacle avoidance, resulting in shortened flight paths and improved transportation timeliness. Thirdly, a cascade sliding mode control scheme is designed for the quadrotor-payload system trajectory tracking under external disturbances. Additionally, a feed-forward controller is designed to effectively suppress the payload's swing. Finally, simulation results shows that the proposed scheme can make the quadrotor-payload system complete the obstacle avoidance task in a short time and on a short path in complex environments, and the designed controller not only has good trajectory tracking performance but also can better suppress external disturbances. In the future, trajectory planning and obstacle avoidance for dynamically moving obstacles in the environment will be further developed as our next research direction of quadrotor-payload system.

REFERENCES

[1] H. Baek and J. Lim, "Design of future UAV-relay tactical data link for reliable UAV control and situational awareness," *IEEE Commun. Mag.*, vol. 56, no. 10, pp. 144–150, Oct. 2018.

[2] A. N. Wilson, A. Kumar, A. Jha, and L. R. Cenkeramaddi, "Embedded sensors, communication technologies, computing platforms and machine learning for UAVs: A review," *IEEE Sensors J.*, vol. 22, no. 3, pp. 1807–1826, Feb. 2022.

[3] I. Sung and P. Nielsen, "Zoning a service area of unmanned aerial vehicles for package delivery services," *J. Intell. Robotic Syst.*, vol. 97, nos. 3–4, pp. 719–731, Mar. 2020.

[4] I. Mademlis, V. Mygdalis, N. Nikolaidis, M. Montagnuolo, F. Negro, A. Messina, and I. Pitas, "High-level multiple-UAV cinematography tools for covering outdoor events," *IEEE Trans. Broadcast.*, vol. 65, no. 3, pp. 627–635, Sep. 2019.

[5] S. Jeong, J. Ko, M. Kim, and J. Kim, "Construction of an unmanned aerial vehicle remote sensing system for crop monitoring," *J. Appl. Remote Sens.*, vol. 10, no. 2, Jun. 2016, Art. no. 026027.

[6] T. H. Pham, D. Ichalal, and S. Mammar, "Complete coverage path planning for pests-ridden in precision agriculture using UAV," in *Proc. IEEE Int. Conf. Netw., Sens. Control (ICNSC)*, Nanjing, China, Oct. 2020, pp. 1–6.

[7] G. Zhang, Y. He, B. Dai, F. Gu, L. Yang, J. Han, and G. Liu, "Aerial grasping of an object in the strong wind: Robust control of an aerial manipulator," *Appl. Sci.*, vol. 9, no. 11, p. 2230, May 2019.

[8] J. Qi, J. Kang, and X. Lu, "Design and research of UAV autonomous grasping system," in *Proc. IEEE Int. Conf. Unmanned Syst. (ICUS)*, Beijing, China, Oct. 2017, pp. 126–131.

[9] Z. Ouyang, R. Mei, Z. Liu, M. Wei, Z. Zhou, and H. Cheng, "Control of an aerial manipulator using a quadrotor with a replaceable robotic arm," in *Proc. IEEE Int. Conf. Robot. Autom. (ICRA)*, Xi'an, China, May 2021, pp. 153–159.

[10] H. Li, Y. Wang, Z. Shi, and M. Chang, "An internal model frame-based disturbance attenuation control scheme for quad-rotors transporting unknown payloads," *Trans. Inst. Meas. Control*, vol. 41, no. 14, pp. 3991–4000, Oct. 2019.

[11] F. Arab, F. A. Shirazi, and M. R. H. Yazdi, "Planning and distributed control for cooperative transportation of a non-uniform slung-load by multiple quadrotors," *Aerosp. Sci. Technol.*, vol. 117, Oct. 2021, Art. no. 106917.

[12] Z.-H. Du, H.-N. Wu, and S. Feng, "Boundary control of a quadrotor UAV with a payload connected by a flexible cable," in *Proc. 37th Chin. Control Conf. (CCC)*, Wuhan, China, Jul. 2018, pp. 1151–1156.

[13] X. Han, R. Miyazaki, T. Gao, K. Tomita, and A. Kamimura, "Controller design and disturbance rejection of multi-quadcopters for cable suspended payload transportation using virtual structure," *IEEE Access*, vol. 10, pp. 122197–122210, 2022.

[14] P. Garcia, R. Lozano, and A. Dzul, *Modelling and Control of Mini-Flying Machines*. New York, NY, USA: Springer-Verlag, Jun. 2005.

[15] M. E. Guerrero, D. A. Mercado, R. Lozano, and C. D. García, "Passivity based control for a quadrotor UAV transporting a cable-suspended payload with minimum swing," in *Proc. 54th IEEE Conf. Decis. Control (CDC)*, Osaka, Japan, Dec. 2015, pp. 6718–6723.

[16] Y. Yang, D. Zhang, H. Xi, and G. Zhang, "Anti-swing control and trajectory planning of quadrotor suspended payload system with variable length cable," *Asian J. Control*, vol. 24, no. 5, pp. 2424–2436, Sep. 2022.

[17] I. H. B. Pizetta, A. S. Brandão, and M. Sarcinelli-Filho, "Load transportation by quadrotors in crowded workspaces," *IEEE Access*, vol. 8, pp. 223941–223951, 2020.

[18] B. Xiao, X. Shengyuan, H. R. Karimi, X. Yu, and Y. Zhang, "Recent developments on advanced safe/reliable control of unmanned systems," *Trans. Inst. Meas. Control*, vol. 41, no. 4, pp. 887–888, Feb. 2019.

[19] B. Ahmed, H. R. Pota, and M. Garratt, "Flight control of a rotary wing UAV using backstepping," *Int. J. Robust Nonlinear Control*, vol. 20, no. 6, pp. 639–658, Apr. 2010.

[20] A. A. Najm and I. K. Ibraheem, "Nonlinear PID controller design for a 6-DOF UAV quadrotor system," 2018, *arXiv:1806.05153*.

[21] Y.-C. Choi and H.-S. Ahn, "Nonlinear control of quadrotor for point tracking: Actual implementation and experimental tests," *IEEE/ASME Trans. Mechatronics*, vol. 20, no. 3, pp. 1179–1192, Jun. 2015.

[22] E. Safwat, Z. Weiguo, M. Kassem, and A. Mohsen, "Robust nonlinear flight controller for small unmanned aircraft vehicle based on incremental backstepping," in *Proc. AIAA Scitech Forum*, Orlando, FL, USA, Jan. 2020.

[23] X. Zhou, R. Liu, J. Zhang, and X. Zhang, "Stabilization of a quadrotor with uncertain suspended load using sliding mode control," in *Proc. 40th Mech. Robot. Conf.*, vol. 5, Charlotte, NC, USA, Aug. 2016.

[24] Z. Wei, Z. Meng, M. Lai, H. Wu, J. Han, and Z. Feng, "Anti-collision technologies for unmanned aerial vehicles: Recent advances and future trends," *IEEE Internet Things J.*, vol. 9, no. 10, pp. 7619–7638, May 2022.

[25] K. Yang, S. K. Gan, and S. Sukkarieh, "An efficient path planning and control algorithm for RUAV's in unknown and cluttered environments," *J. Intell. Robotic Syst.*, vol. 57, nos. 1–4, pp. 101–122, Jan. 2010.

[26] G. Farid, S. Cocuzza, T. Younas, A. A. Razzaqi, W. A. Wattoo, F. Cannella, and H. Mo, "Modified A-star (A*) approach to plan the motion of a quadrotor UAV in three-dimensional obstacle-cluttered environment," *Appl. Sci.*, vol. 12, no. 12, p. 5791, Jun. 2022.

[27] D. Zhang, Y. Yang, H. Han, and Y. Hu, "Binocular visual pendulum angle detection and anti-swing control of quadrotor suspension system," *SSRN Electron. J.*, vol. 45, no. 4, pp. 723–735, Feb. 2022.

[28] O. Khatib, "Real-time obstacle avoidance for manipulators and mobile robots," *Int. J. Robot. Res.*, vol. 5, no. 1, pp. 90–98, Mar. 1986.

[29] O. Montiel, U. Orozco-Rosas, and R. Sepúlveda, "Path planning for mobile robots using bacterial potential field for avoiding static and dynamic obstacles," *Expert Syst. Appl.*, vol. 42, no. 12, pp. 5177–5191, Jul. 2015.

[30] N. Wang, J. Dai, and J. Ying, "UAV formation obstacle avoidance control algorithm based on improved artificial potential field and consensus," *Int. J. Aeronaut. Space Sci.*, vol. 22, no. 6, pp. 1413–1427, Dec. 2021.

[31] J. Kang, Z. Huang, and H. Wen, "Trajectory optimization with switchable encpsulating circle for quadrotor carrying slang payload," *J. Dyn. Control*, vol. 19, no. 4, pp. 73–80, 2021.

[32] X. Dai, Q. Quan and S. Wang, *Multicopter Design and Control Practice: A Series Experiments based on MATLAB and Pixhawk*. Springer, Apr. 2020.

[33] V. L. Rvachev and T. I. Sheiko, "R-functions in boundary value problems in mechanics," *Appl. Mech. Rev.*, vol. 48, no. 4, pp. 151–188, Apr. 1995.

[34] Y. Du, X. Zhang, and Z. Nie, "A real-time collision avoidance strategy in dynamic airspace based on dynamic artificial potential field algorithm," *IEEE Access*, vol. 7, pp. 169469–169479, 2019.

[35] X. Yuan, "Research on the limitations of UAV path planning based on artificial potential field method," in *Proc. 9th Int. Forum Electr. Eng. Autom. (IFEEA)*, Zhuhai, China, Nov. 2022, pp. 619–622.

[36] Y. Luo, X. Huang, C. Wu, and S. Leng, "Enhanced artificial potential field-based moving obstacle avoidance for UAV in three-dimensional environment," in *Proc. IEEE 16th Int. Conf. Control Autom. (ICCA)*, Singapore, Oct. 2020, pp. 177–182.

[37] D. Shi, Z. Wu, and W. Chou, "Generalized extended state observer based high precision attitude control of quadrotor vehicles subject to wind disturbance," *IEEE Access*, vol. 6, pp. 32349–32359, 2018.

ZIYOU ZHANG received the B.S. degree in automation from the Qingdao University of Technology, Qingdao, China, in 2017, where he is currently pursuing the M.S. degree with the School of Information and Control Engineering. His research interests include modeling and control of robots, and trajectory planning.

DONG ZHANG received the M.S. and Ph.D. degrees in control theory and control engineering from Shandong University, China, in 2006 and 2009, respectively. He is currently a Professor with the School of Information and Control Engineering, Qingdao University of Technology, China. His current research interests include nonlinear control systems, robotics, and intelligent control.

DEZHI KONG received the B.S. degree in electrical engineering and automation from the Qingdao University of Technology, Qingdao, China, in 2017, where he is currently pursuing the M.S. degree with the School of Information and Control Engineering. His research interests include robot control and event-triggered control.

YANQIAN WANG received the B.S. degree in automation from Dalian Jiaotong University, Dalian, China, in 2002, the M.S. degree in control theory and control engineering from the Shaanxi University of Science and Technology, Xi'an, China, in 2005, and the Ph.D. degree in control science and engineering from the Nanjing University of Science and Technology, Nanjing, China, in 2015. He was a Postdoctoral Fellow with the University of South Florida, from 2015 to 2016. Since March 2018, he has been with the School of Information and Control Engineering, Qingdao University of Technology, Qingdao, China, where he is currently an Associate Professor. His research interests include robust control and filtering, singular systems, stochastic systems, and cyber physical systems.